Tetrahedron 68 (2012) 9672–9678

Contents lists available at SciVerse ScienceDirect

Tetrahedron

journal homepage: www.elsevier.com/locate/tet

Synthesis of new bipolar materials based on diphenylphosphine oxide and triphenylamine units: efficient host for deep-blue phosphorescent organic light-emitting diodes

Wei Jiang[a], Wen Yang[a], Xinxin Ban[a], Bin Huang[a], Yunqian Dai[a], Yueming Sun[a,*], Lian Duan[b,*], Yong Qiu[b]

[a] School of Chemistry and Chemical Engineering, Southeast University, Nanjing, Jiangsu 211189, PR China
[b] Department of Chemistry, Tsinghua University, Beijing 100084, PR China

ARTICLE INFO

Article history:
Received 26 June 2012
Received in revised form 25 August 2012
Accepted 11 September 2012
Available online 16 September 2012

Keywords:
Triphenylamine
Bipolar
Solution processed
High triplet energy
Host
Phosphorescence

ABSTRACT

This paper reports the synthesis and physical properties of a series of bipolar host materials, using of a hole-transporting triphenylamine (TPA) monomer as a core incorporated with different numbers of diphenylphosphine oxide (PO) as electron-transporting moieties, 4-(diphenylphosphoryl)-*N*,*N*-diphenylaniline (DDPA), 4-(diphenylphosphoryl)-*N*-(4-(diphenylphosphoryl)phenyl)-*N*-phenylaniline (DDPP), and tris(4-(diphenylphosphoryl)phenyl)amine (TDPA), for solution-processed deep-blue phosphorescent organic light-emitting devices (PhOLEDs). With the increasing numbers of PO units, the glass-transition temperature of those compounds rise gradually. Moreover, the newly synthesized compounds all possess high triplet energies, which can prevent back energy transfer between the host and dopant molecules, and are expected to serve as appropriate hosts for iridium(III) tris(3,5-difluoro-4-cyanophenyl)pyridinato-N,C′ (FCNIrpic). The solution-processed devices using DDPP and TDPA as the hosts for the phosphorescence emitter FCNIrpic showed the maximum luminance efficiencies of 9.7 and 6.6 cd A^{-1}, respectively. The efficiency of TDPA based device shows nearly three times higher than the value of commonly used host material 1,3-bis(9-carbazolyl)benzene (mCP) with the same structure, which is outstanding with respect to other works related to the solution-processed deep-blue PhOLEDs based on small-molecule hosts.

1. Introduction

Phosphorescent organic lighting-emitting diodes (PhOLEDs) have attracted a great deal of attention because they can harvest singlet and triplet excitons for emission, theoretically yielding 100% internal quantum efficiency, which show great applicable in full-color flat-panel displays and solid-state lighting sources.[1–5] Recently, in order to simplify the fabrication process of PhOLEDs and reduce the cost of larger-area displays, much research effort has been devoted to develop highly efficient PhOLEDs with the emitting layer prepared by solution-processing techniques. For example, Doh et al. used small-molecule mixed host in the solution-processed blue-PhOLEDs and reported high external quantum efficiency (EQE) of 14.6%.[6] Zhao et al. has recently reported green PhOLEDs using a solution-processed polyethyleneoxide (PEO) hole blocking layer and a Cs_2CO_3/Al cathode, which gave a maximum luminous efficiency (LE) of 32.1 cd A^{-1}.[7] Yang et al. reported highly efficient red PhOLEDs based on a solution-processable bipolar host with a maximum LE value of 13.3 cd A^{-1}.[8] While red, green, and sky-blue PhOLEDs fabricated by solution processing have been developed with obvious progress, high performance solution-processed deep-blue PhOLEDs are still scarce, owing to lack of the appropriate host materials. As an effective host for deep-blue PhOLEDs, its triplet energy requires to be larger than that of the phosphorescent emitters such as FCNIrpic (2.74 eV) and iridium(III) bis(4′,6′-difluorophenylpyridinato)tetrakis(1-pyrazolyl)borate (FIr6) (2.72 eV) to prevent the reverse energy transfer from the dopant.[9,10]

During the search for host materials for solution-processed PhOLEDs, a great deal of attention has been focused on polymer-based materials, owing to their early access to solution-processing strategy.[11,12] However, the impurities in polymer materials could result in exciton quenching and device failure. In contrast to polymer counterparts, small-molecule materials are advantageous as they have defined molecular structure, definite molecular weight, high purity, and easy purification.[13–19]

---

* Corresponding authors. Tel./fax: +86 25 52090621; e-mail addresses: 101011462@seu.edu.cn (Y. Sun), duanl@tsinghua.edu.cn (L. Duan).

0040-4020/$ – see front matter © 2012 Elsevier Ltd. All rights reserved.
http://dx.doi.org/10.1016/j.tet.2012.09.051

Nowadays, bipolar hosts have potential advantages arising from more balanced injection and transport of holes and electrons, which may result in a broad distribution of recombination region within the emitting layer and a low efficiency roll-off of the devices.[20–28] One of approach to the design of bipolar host materials is to combine reported hole-transporting and electron-transporting functional units. Triphenylamine (TPA) and diphenylphosphine oxide (PO) have been regarded as promising moieties for organic semiconductor materials owing to their hole and electron transport properties.[29–35] Furthermore, the π conjugation of the molecules was interrupted by the insertion of P=O moieties, which resulted in high triplet energy for molecules. Padmaperuma et al. reported highly efficient blue PhOLEDs with an bipolar host material 4-(diphenylphosphoryl)-*N*,*N*-diphenylaniline (DDPA) (see Scheme 1), which gave a maximum EQE of 17.1%.[36] However, the DDPA suffers from poor thermal stability with a low glass-transition temperatures (T_g=51 °C) (see Fig. 1b) and may result in phase segregation and aggregation in the device.

The bipolar host materials containing carbazole and PO units are nowadays widely investigated. However, few reported work has focused on TPA-based PO bipolar host material. In this paper, we synthesized two small-molecule based host materials, 4-(diphenylphosphoryl)-*N*-(4-(diphenylphosphoryl)phenyl)-*N*-phenylaniline (DDPP) and tris(4-(diphenylphosphoryl)phenyl)amine (TDPA), using a hole-transporting TPA monomer as a core incorporated with different numbers of PO as electron-transporting moieties. The influence of the PO moieties on the thermal stability, electrochemical properties, photophysical behaviors, and EL performances of those bipolar host materials are investigated.

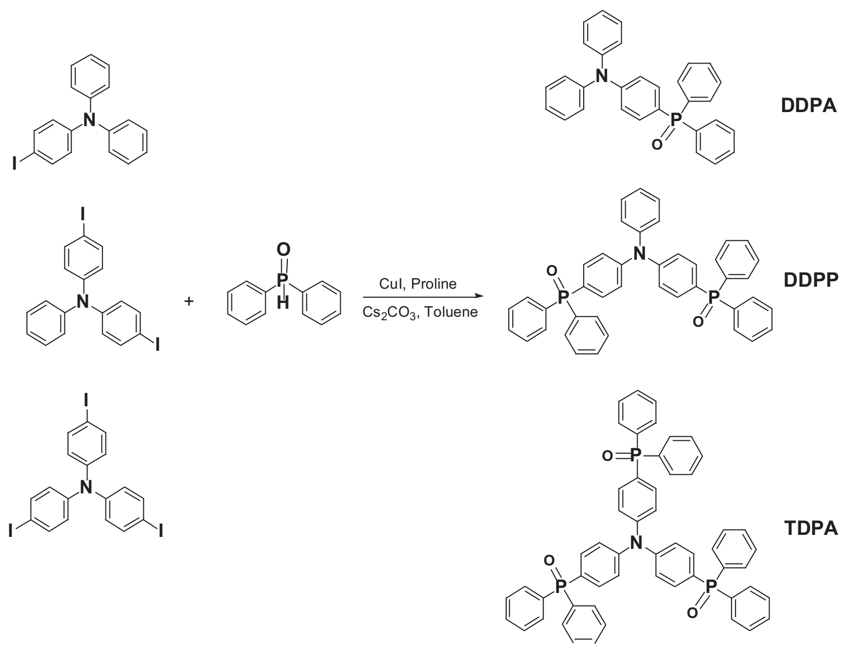

Scheme 1. Synthetic routes toward DDPA, DDPP, and TDPA.

2. Experimental

2.1. General information

All reactants and solvents, unless otherwise stated, were purchased from commercial sources and used as received. ^{1}H NMR and ^{13}C HMR spectra were measured on a Bruker ARX300 NMR spectrometer with tetramethylsilane as the internal standard. Elemental analysis was performed on an Elementar Vario EL CHN elemental analyzer. Mass spectrometry was performed with a Thermo Electron Corporation Finnigan LTQ mass spectrometer. Absorption spectra were recorded with an UV–vis spectrophotometer (Shimadzu UV-2450) and PL spectra were recorded with a fluorospectrophotometer (Jobin Yvon, FluoroMax-3). TGA was recorded with a Netzsch simultaneous thermal analyzer (STA) system (STA 409PC) under a dry nitrogen gas flow at a heating rate of 10 °C min^{-1}. Glass-transition temperatures were recorded by DSC at a heating rate of 10 °C min^{-1} with a thermal analysis instrument (DSC 2910 modulated calorimeter). Cyclic voltammetry was performed on a Princeton Applied Research potentiostat/galvanostat model 283 voltammetric analyzer in CH_2Cl_2 solutions (10^{-3} M) at a scan rate of 100 mV s^{-1} with a platinum plate as the working electrode, a silver wire as the pseudo-reference electrode, and a platinum wire as the counter electrode. The supporting electrolyte was tetrabutylammonium hexafluorophosphate (0.1 M) and ferrocene was selected as the internal standard. The solutions were bubbled with argon for 10 min before measurements. The film surface morphology was measured with AFM (Seiko Instruments, SPA-400).

2.2. Device fabrication and performance measurements

In a general procedure, indium-tin oxide (ITO)-coated glass substrates were pre-cleaned carefully and treated by UV ozone for 4 min. A 40 nm poly(3,4-ethylenedioxythiophene)doped with poly(styrene-4-sulfonate) (PEDOT:PSS) aqueous solution was spin coated onto the ITO substrate and baked at 200 °C for 10 min. The substrates were then taken into a nitrogen glove box, where FCNIrpic-doped host layer was spin coated onto the PEDOT:PSS layer from 1,2-dichloroethane solution and annealed at 80 °C for 30 min. The substrates were then transferred into an evaporation chamber, where the TPBI was evaporated at an evaporation rate of 1–2 A/s under a pressure of 4×10^{-4} Pa and the Cs_2CO_3/Al bilayer

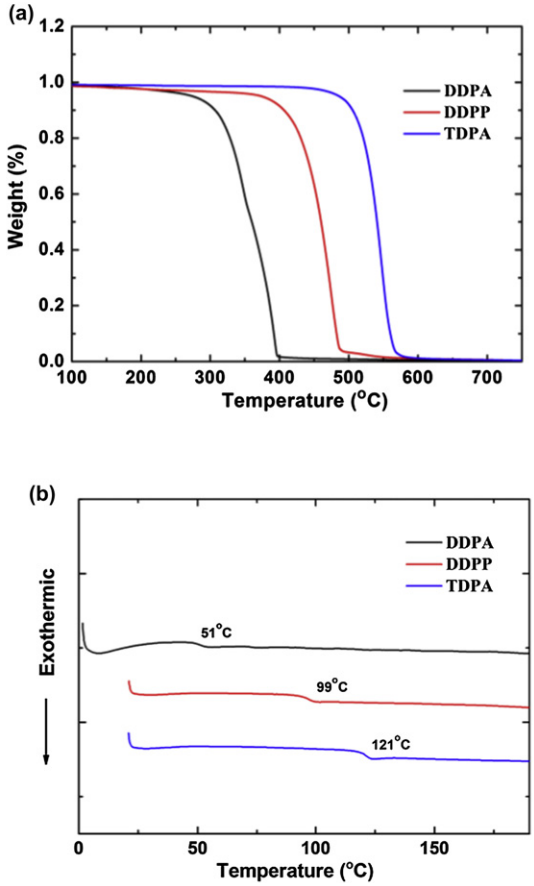

Fig. 1. (a) TGA traces of DDPA, DDPP, and TDPA recorded at a heating rate of 10 °C min^{-1}. (b) DSC measurement recorded at a heating rate of 10 °C min^{-1}.

cathode was evaporated at evaporation rates of 0.2 and 10 A/s for Cs_2CO_3 and Al, respectively, under a pressure of 1×10^{-3} Pa. The current–voltage–brightness characteristics of the devices were characterized with Keithley 4200 semiconductor characterization system. The electroluminescent spectra were collected with a Photo Research PR705 Spectrophotometer. All measurements of the devices were carried out in ambient atmosphere without further encapsulations.

2.3. Materials

2.3.1. Synthesis of 4-(diphenylphosphoryl)-N,N-diphenylaniline (DDPA). A mixture of (4-iodo-phenyl)-diphenylamine (1.0 mmol), diphenylphosphine oxide (1.2 mmol), CuI (0.10 mmol), proline (0.10 mmol), and Cs_2CO_3 (1.5 mmol) was added to toluene solution (20 mL). The mixture was heated under reflux for 24 h. After the reaction finished, the reaction mixture was extracted with dichloromethane and washed with water. The organic layer was dried by anhydrous $MgSO_4$ and filtered. The product was isolated by silica gel column chromatography using methanol/ethyl acetate (1:20) as eluent to afford an oyster white solid (0.25 g, 56.2%). ^{1}H NMR (300 MHz, $CDCl_3$, TMS) δ: 7.71 (d, J=6.9 Hz, 2H), 7.67 (d, J=6.9 Hz, 2H), 7.57–7.37 (m, 9H), 7.05–6.96 (m, 2H), 7.31 (t, J=7.2 Hz, 4H), 7.14–7.09 (m, 5H); C NMR ($CDCl_3$, δ): 133.2, 133.1, 132.0, 131.7, 129.6, 128.4, 128.3, 125.8, 125.68, 124.4, 120.3, 120.2; (MALDI-TOF) [m/z]: calcd for $C_{30}H_{24}NOP$, 445.5; found, 445.1. Anal. Calcd for $C_{30}H_{24}NOP$: C, 80.88; H, 5.43; N 3.14. Found: C, 80.66; H, 5.32; N 3.25.

2.3.2. Synthesis of 4-(diphenylphosphoryl)-N-(4-(diphenylphosphoryl)phenyl)-N-phenylaniline (DDPP). A mixture of bis-(4-iodo-phenyl)-phenylamine (1.0 mmol), diphenylphosphine oxide (2.4 mmol), CuI (0.20 mmol), proline (0.20 mmol), and Cs_2CO_3 (3.0 mmol) was added to toluene solution (20 mL). The mixture was heated under reflux for 24 h. After the reaction finished, the reaction mixture was extracted with dichloromethane and washed with water. The organic layer was dried by anhydrous $MgSO_4$ and filtered. The product was isolated by silica gel column chromatography using methanol/ethyl acetate (1:10) as eluent to afford an oyster white solid (0.29 g, 45.1%). ^{1}H NMR (300 MHz, $CDCl_3$, TMS) δ: 7.69 (d, J=6.9 Hz, 4H), 7.65 (d, J=6.9 Hz, 4H), 7.53–7.40 (m, 16H), 7.32 (t, J=7.2 Hz, 2H), 7.13–7.07 (m, 7H); C NMR ($CDCl_3$, δ): 133.4, 133.3, 132.1, 132.0, 131.9, 129.9, 128.5, 128.4, 126.7, 125.5, 122.6, 122.5; MS (MALDI-TOF) [m/z]: calcd for $C_{42}H_{33}NO_2P_2$, 645.7; found, 645.3. Anal. Calcd for $C_{42}H_{33}NO_2P_2$: C, 78.13; H, 5.15; N 2.17. Found: C, 78.40; H, 4.99; N 2.25.

2.3.3. Synthesis of tris(4-(diphenylphosphoryl)phenyl)amine (TDPA). A mixture of tris-(4-iodo-phenyl)-amine (1.0 mmol), diphenylphosphine oxide (3.6 mmol), CuI (0.30 mmol), proline (0.30 mmol), and Cs_2CO_3 (4.5 mmol) was added to toluene solution (20 mL). The mixture was heated under reflux for 36 h. After the reaction finished, the reaction mixture was extracted with dichloromethane and washed with water. The organic layer was dried by anhydrous $MgSO_4$ and filtered. The product was isolated by silica gel column chromatography using methanol/ethyl acetate (1:5) as eluent to afford an oyster white solid (0.30 g, 35.5%). ^{1}H NMR (300 MHz, $CDCl_3$, TMS) δ: 7.71 (d, J=8.2 Hz, 4H), 7.67 (t, J=6.9 Hz, 4H), 7.60–7.37 (m, 16H), 7.31–7.26 (m, 6H), 7.14 (t, J=7.2 Hz, 8H), 7.02–6.98 (m, 4H); C NMR ($CDCl_3$, δ): 133.8, 133.7, 133.2, 132.1, 132.0, 128.7, 128.5, 127.7, 124.1, 124.0; MS (MALDI-TOF) [m/z]: calcd for $C_{54}H_{42}NO_3P_3$, 845.8; found, 845.4. Anal. Calcd for $C_{54}H_{42}NO_3P_3$: C, 80.88; H, 5.43; N 3.14. Found: C, 80.66; H, 5.32; N 3.25.

3. Results and discussion

3.1. Synthesis and morphological stability

Generally, the PO derivatives can be synthesized by coupling reactions between lithiated intermediates and diphenylchlorophosphine followed by oxidation with hydrogen peroxide. In this paper, the target compounds were synthesized by the commonly Ullmann coupling reaction. Scheme 1 illustrates the synthetic procedures for DDPA, DDPP, and TDPA. Initially, the starting (4-iodo-phenyl)-diphenylamine, bis-(4-iodo-phenyl)-phenylamine and tris-(4-iodo-phenyl)-amine were synthesized according to methods previously described and then reacted with diphenylphosphine oxide led to DDPA, DDPP, and TDPA in the presence of CuI/proline with moderate yields, respectively. As shown in Experimental section, the yield decreases with increasing numbers of PO. The target compounds were purified by silica column method and recrystallization, producing very pure powders. H NMR, C NMR, mass spectrometry, and elemental analysis were employed to confirm the chemical structures of above-mentioned compounds as described in Experimental section. The thermal and morphological stability of DDPA, DDPP, and TDPA were also investigated by thermal gravimetric analyses (TGA) and differential scanning calorimetry (DSC) (Fig. 1). These compounds possess thermal decomposition temperature (T_d, corresponding to 5% weight loss) ranging from 275 to 486 °C. They are all readily formed a glass from their melts upon fast cooling, and the glass-transition temperature (T_g) range from 51 to 121 °C. It was found that the T_g and T_d of those compounds rose gradually with the increasing numbers of PO units. The T_g of DDPP and TDPA is much higher than commonly used host materials such as 4,4′-bis(9-carbazolyl)-2,2′-biphenyl (CBP) (62 °C) and mCP (55 °C). The observed low T_g of DDPA demonstrates the high tendency to crystallize in the operated devices. Compared to DDPA, DDPP and TDPA show significantly rises of the T_d and T_g values by introducing additional numbers of PO groups. The better thermal performance of DDPP and TDPA is attributed to the tetrahedral geometry of PO, which effectively hinders the molecule packing and crystallization. The Atomic force microscopy (AFM) results indicate the excellent thermal and morphological stability of these compounds (Supplementary data Fig. S1). Therefore, DDPP and TDPA are advantageous in the film morphology stability, which will suppress the phase separation during device operation.

3.2. Theoretical calculations

To further understand the relationship of the electronic properties at molecular level, density functional theory (DFT) calculations were carried out using B3LYP hybrid functional theory with 6-31G* basis sets. As can be seen from Fig. 2, the calculated geometries of DDPA, DDPP, and TDPA show that the tetrahedral geometry of PO units is significantly twisted against to the TPA core, resulting in a non-planar structure in each molecule. These geometrical characteristics are beneficial to the amorphous of the organic compounds and, thus, suppress molecular recrystallization, which are in agreement with the TGA and DSC results. Furthermore, the tetrahedral geometry of PO moieties interrupted the extent of conjugation between the central core and branches, which keeps the triplet energy gap at a high level of these molecules. Their triplet energies are calculated from the difference of their ground state and triplet excited state energies. The calculated triplet energies ΔE (T_1–S_0) of TPA, DDPA, DDPP, and TDPA are 3.18, 3.03, 2.89, and 2.85 eV, and it further proves that insertion of PO moieties as the branches in combination of TPA leads to desirable high triplet energy, which are high enough to serve as hosts for blue triplet emitters.

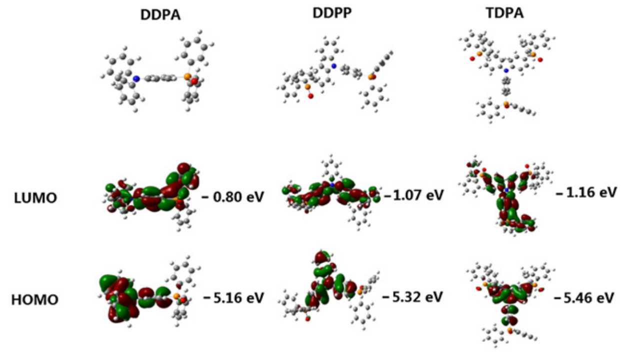

Fig. 2. Optimized geometries and calculated HOMO and LUMO density maps for DDPA, DDPP, and TDPA according to DFT calculations at B3LYP/6-31* level.

Calculated HOMO and LUMO density maps of DDPA, DDPP, and TDPA are also included in Fig. 2. Compared with TPA core (HOMO=−4.94 eV), the HOMO levels of DDPA, DDPP, and TDPA increase (from −5.16 to −5.46 eV) with the increasing numbers of PO units, while the LUMO levels move down (from −0.80 to −1.16 eV). As a result, the HOMO–LUMO energy gaps become narrow (from 4.25 to 4.36 eV). HOMOs of all compounds are mainly located at the hole-transporting TPA moieties. In contrast, their LUMOs mostly correspond to the lowest π-orbital of the periphery triphenyl phosphine oxide moiety. It is interesting to note that all molecules show significant separation in the spatial distributions between HOMO and LUMO at their different moieties, which is believed to facilitate the balance carrier injecting/transporting.[25]

3.3. Electrochemical analysis

The electrochemical properties of DDPA, DDPP, and TDPA were studied in solution using cyclic voltammetry (CV) using tetrabutylammonium hexafluorophosphate($TBAPF_6$) as the supporting electrolyte and ferrocene as the internal standard. As shown in Fig. 3, during the anodic scan in dichloromethane, DDPA, DDPP, and TDPA exhibited similar quasi-reversible oxidation process, which can be assigned to the oxidation of electron-donating TPA moiety, with onset potentials of 0.86, 1.05, and 1.25 V, respectively. No reduction waves were detected. On the basis of the onset potentials for oxidation, we estimated the HOMO energy of DDPA, DDPP, and TDPA to be −5.30, −5.49, and −5.69 eV. These results reveal that the introduction of PO groups to the TPA core can lead to the raising of HOMO levels, which are in agreement with the DFT calculations results. These together with absorption spectra were then used to obtain the LUMO energy levels.

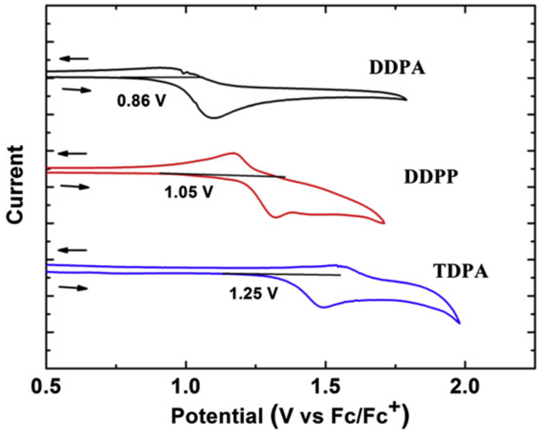

Fig. 3. The CV curves of DDPA, DDPP, and TDPA in CH_2Cl_2 solutions (10^{-3} M).

3.4. Photophysical properties

Fig. 4 depicts the UV–vis absorption and photoluminescent (PL) spectra of DDPA, DDPP, and TDPA in dilute CH_2Cl_2 solutions. The absorption spectra of three PO compounds are similar, which show peaks at around 230 nm could be assigned to the n–π^* transitions of TPA moiety, while the longer-wavelength absorptions from 323 to 339 nm could be attributed to π–π^* transitions from TPA moiety to PO moiety. Compared to DDPA, the absorption maxima of DDPP and TDPA are red-shifted by 16 and 12 nm, respectively. The PL emission of DDPA, DDPP, and TDPA exhibits peaks at 408, 388, and 379 nm, respectively. The hypochromatic shift of the PL spectrum is clearly found by introducing PO moiety, and the more PO moieties present in the TPA core, the larger hypochromatic shift obtained. This phenomenon may be attributed to the symmetrical geometry of DDPP and TDPA, which lead to the decreasing of the magnitude of the change in the dipole moment from the ground state to the excited state ($\Delta\mu$) and weaken the intramolecular charge transfer (ICT) effect. The band gap was calculated from the edge of the UV–vis absorption peak, giving values of 3.49, 3.41, and 3.43 eV for DDPA, DDPP, and TDPA, respectively. The highest energy 0–0 phosphorescent emission was used to calculate the triplet energy level, giving a value of 2.78 eV for DDPA, 2.80 eV for DDPP, and 2.85 eV for TDPA, higher than the values of the commonly used triplet blue-emitter FIrpic (2.62 eV) and FCNIrpic (2.74 eV). Inconsistent with the calculation results, ΔE (T_1-S_0) of DDPA with one PO moiety is the smallest one among these hosts, and larger ΔE (T_1–S_0) is

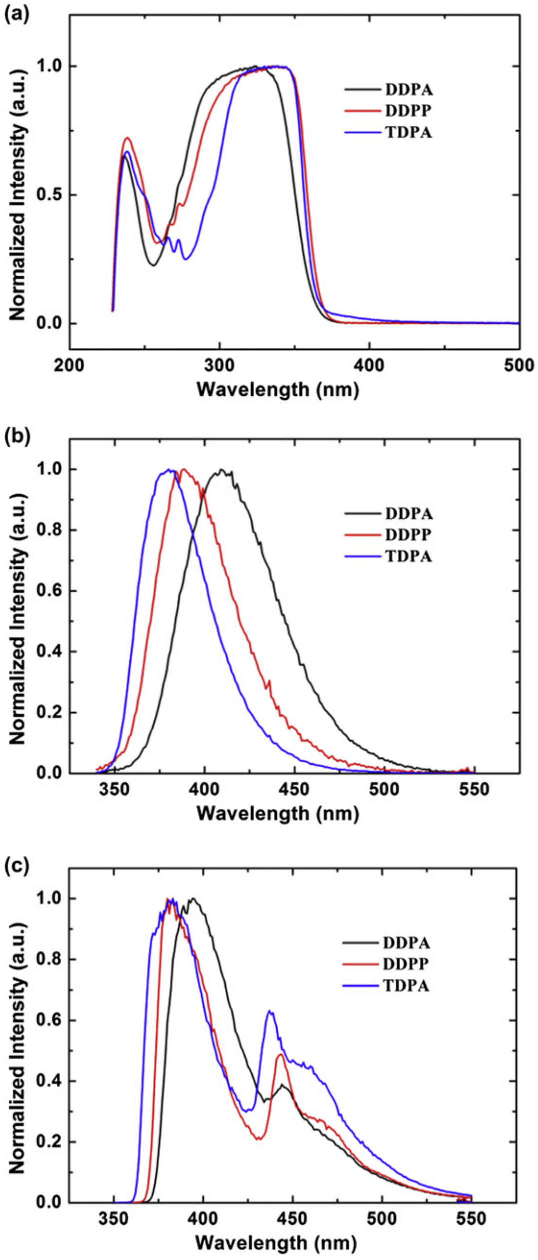

Fig. 4. Normalized absorption (a), emission (b), and phosphorescence (77 K) spectra (c) of DDPA, DDPP, and TDPA in dilute solutions.

achieved with introducing more PO moieties to TPA core. Using host materials that possess high triplet energies is a provision for effective confinement of the triplet excitons on the guest and, consequently, prevention of back energy transfer between the host and dopant molecules. Based on the results of the measurements, the newly synthesized compounds with high triplet energy levels are expected to serve as appropriate hosts for FCNIrpic.

To gain more insight fluorescence spectra of the systems were recorded in various solvents of different polarity. As shown in Table 1, a red-shift is observed for solutions with solvents of increasing polarity. As a change of the solvent from *n*-hexane to acetonitrile (ACN), the maximum emission wavelengths were red-shifted from 363 to 423 nm, 369 to 400 nm, and 368 to 384 nm for DDPA, DDPP, and TDPA, respectively. The large Stokes shift for DDPA in polar solvents as compared to non-polar solvents indicating a considerable energetic stabilization of the excited state in polar solvents. Such results indicated that the molecular dipole moments of these compounds are different from each other. To obtain more information about the change in the dipole moment upon excitation, we used the Lippert–Mataga equation Eq. 1,[37] which expressed the Stokes shift as a function of the solvent polarity parameter $\Delta f(\varepsilon,n)$.

Table 1
Photophysical properties of the hosts in various solvents

Solvents	Δf	$\lambda_{\text{max,abs}}$ (nm)			λ_{em} (nm)		
		DDPA	DDPP	TDPA	DDPA	DDPP	TDPA
n-Hexane	0.001	314	334	330	363	369	368
THF	0.207	316	336	333	400	384	374
CH_2Cl_2	0.218	323	339	335	409	388	379
ACN	0.306	318	336	332	423	400	384

$$\upsilon_a - \upsilon_a = \frac{2\Delta\mu^2}{hca^3}\Delta f(\varepsilon,n) + C = 10070\Delta\mu^2\frac{\Delta f(\varepsilon,n)}{a^3} + C \tag{1}$$

where $\Delta f(\varepsilon,n)$ is calculated from Eq. 2:

$$\Delta f(\varepsilon,n) = \left[\frac{\varepsilon-1}{2\varepsilon+1} - \frac{n^2-1}{2n^2+1}\right] \tag{2}$$

In these relations, $\nu_a - \nu_f$ represents the Stokes shift (in cm^{-1}), where υ_a and υ_f are the spectral positions of the absorption maximum and solvent-equilibrated fluorescent maximum, respectively. $\Delta\mu$ is given by $\mu_e - \mu_g$, which is the magnitude of the change in the dipole moment from the ground state to the excited state. The other terms are: h corresponds to the Planck's constant (6.6×10^{-34} J s), c is the velocity of light in the vacuum (3.0×10^8 m s^{-1}) and a is the Onsager cavity radius (in meter), respectively. Onsager cavity radius was estimated from the optimized distance between the two farthest atoms in the direction of charge separation within the molecule. Δf is the orientation polarizability parameter of the solvent where n is the refractive index of the medium and ε is the static dielectric constant of the solvent (both at room temperature). The Lippert–Mataga plot for DDPA, DDPP, and TDPA is shown in Fig. 5. From the slope of this plot, the difference of the dipole moment between the excited state and the ground state is estimated to be 15.2, 10.65, and 8.1 D for DDPA, DDPP, and TDPA, respectively. It was found that the $\Delta\mu$ values of those compounds decrease gradually with the increasing numbers of PO units. The calculated $\Delta\mu$ of DDPA is much larger than DDPP and TDPA, which is typical for photoinduced intramolecular charge transfer (ICT) processes. It was reported that EL and consequently the performance of OLEDs are strongly affected by the molecular dipole moment. The

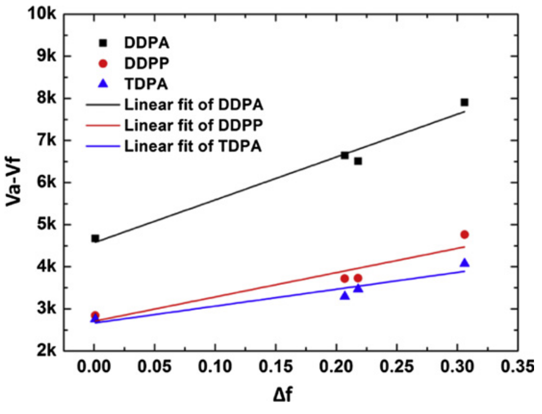

Fig. 5. Lippert–Mataga plot of DDPA, DDPP, and TDPA in various solutions.

intramolecular and intermolecular electric field arising from the molecular dipoles is a detrimental factor that should be avoided in the molecular design of high performance OLEDs.

3.5. Electroluminescent properties

The high triplet energy for those new compounds makes it a good candidate as solution-processed hosts for deep-blue phosphorescent emitters such as FCNIrpic. To investigate the function of those compounds in deep-blue PhOLEDs, we fabricated double-layer deep-blue electrophosphorescent devices with DDPP and TDPA as hosts and 10 wt % FCNIrpic as the dopant. The device with the configuration ITO/PEDOT:PSS/Host:FCNIrpic(10 wt %)//TPBi/Cs_2CO_3/Al has been fabricated by spin-coating. The material structures and the energy-level diagrams of the device are shown in Fig. 6. We used conducting polymer PEDOT:PSS as a hole-injection layer, TPBi as an electron-transporting layer, and Cs_2CO_3 as the electron-injection layer. The current density–voltage–luminance (*I*–*V*–*L*) and luminous efficiency–luminance (*LE*–*L*) characteristics are shown in Fig. 7. By using DDPP and TDPA, devices showed the turn-on voltage (corresponding to 1 cd m^{-2}) of 6.0 and 6.2 V, respectively. The device based on TDPA shows better performance with the maximum LE value of 9.7 cd A^{-1}, and the maximum EQE of 5.7%, while the maximum luminance efficiencies of DDPP based device was 6.6 cd A^{-1}, and the corresponding external quantum efficiency was 3.9%. The efficiency of TDPA based solution-processed deep-blue PhOLEDs shows nearly three times higher than the values of mCP with the maximum LE value of 3.6 cd A^{-1} and EQE of 2.0% for the same device,[17] which was comparable to the literature value reported by Yang's group,[19] with the maximum LE value of 12.5 cd A^{-1}. The excellent performance is probably due to the excellent thermal stability of the DDPP and TDPA, which significantly enhances the capability of forming stable amorphous thin films. In addition, the bipolar charge transport nature of DDPP and TDPA that increases carrier balance in the emitting layer may also contribute to the high performance. As shown in Fig. 7b, the electroluminescence (EL) spectra of the devices are almost identical with the CIE coordinates of (0.18, 0.24), corresponding to the emission of FCNIrpic. Furthermore, no additional emission coming from host materials was observed, indicative of efficient energy transfer from the host to FCNIrpic.

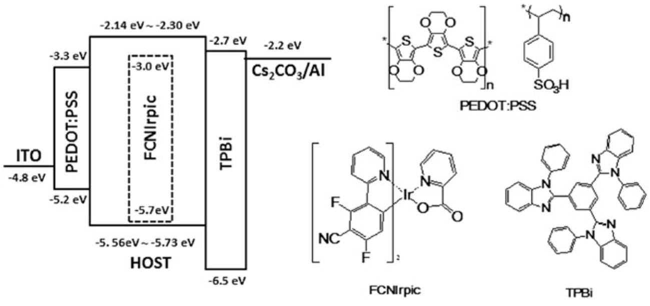

Fig. 6. Structures of the materials in the devices and the energy-level diagrams.

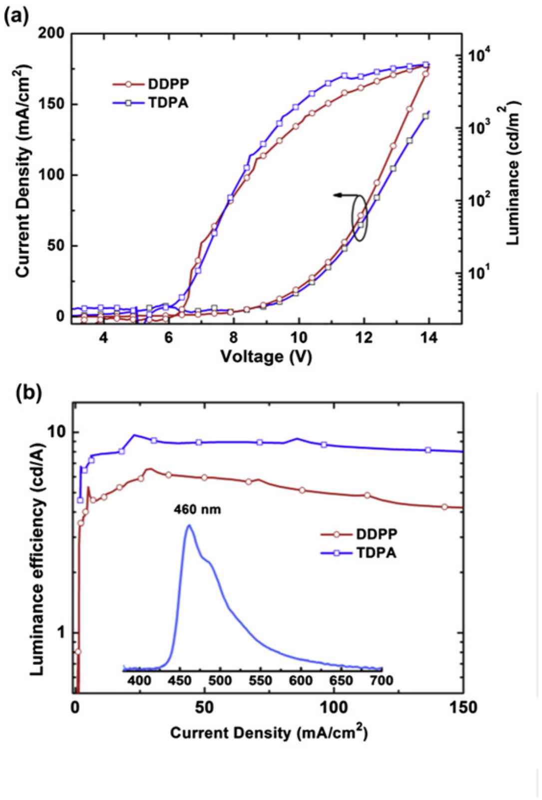

Fig. 7. Comparison of device characteristics (a) luminance–voltage–current density, (b) luminance efficiency–current density, inset: EL spectrum.

4. Conclusions

In summary, we have designed and synthesized two new bipolar host materials DDPP and TDPA for solution-processed deep-blue PhOLEDs. Owing to their unique structural feature, different numbers of PO units substituted TPA derivatives exhibit the excellent thermal stability and provide high triplet energy. In addition, it was found that the $\Delta\mu$ values of those compounds decrease gradually with the increasing numbers of PO units, which is beneficial to improve device performance. Utilizing those compounds as host materials, the solution-processed deep-blue phosphorescence OLEDs with FCNIrpic as a dopant show a maximum current efficiency of 9.7 cd A^{-1}, which is outstanding with respect to other works based on small-molecule hosts.

Acknowledgements

This work was supported by the National Natural Science Foundation of China (grant nos. 51103023 and 21173042).

Supplementary data

Supplementary data associated with this article can be found in the online version, at http://dx.doi.org/10.1016/j.tet.2012.09.051.

References and notes

1. Tang, C. W.; Vanslyke, S. A. *Appl. Phys. Lett.* **1987**, *51*, 913.
2. Forrest, S. R. *Nature* **2004**, *428*, 911.
3. Wu, C. C.; Lin, Y. T.; Wong, K. T.; Chen, R. T.; Chien, Y. Y. *Adv. Mater.* **2004**, *16*, 61.
4. Heeger, A. J. *Angew. Chem., Int. Ed.* **2001**, *40*, 2591.
5. Reineke, S.; Lindner, F.; Schwartz, G.; Seidler, N.; Lüeesem, B.; Leo, K. *Nature* **2009**, *459*, 234.
6. Doh, Y. J.; Park, J. S.; Jeon, W. S.; Pode, R.; Kwon, J. H. *Org. Electron.* **2012**, *13*, 586.
7. Zhao, Y.; Duan, L.; Zhang, D. Q.; Hou, L. D.; Qiao, J.; Wang, L. D.; Qiu, Y. *Appl. Phys. Lett.* **2012**, *100*, 088304.
8. Zhu, M. R.; Ye, T. L.; He, X.; Cao, X. S.; Zhong, C.; Ma, D. G.; Qin, J. G.; Yang, C. L. *J. Mater. Chem.* **2011**, *21*, 9326.
9. Yook, K. S.; Lee, J. Y. *Org. Electron.* **2011**, *21*, 1711.
10. Holmes, R. J.; D'Andrade, B. W.; Forrest, S. R.; Ren, X.; Li, J.; Thompson, M. E. *Appl. Phys. Lett.* **2003**, *83*, 3818.
11. Liu, J.; Pei, Q. B. *Macromolecules* **2010**, *43*, 9608.
12. Liu, J.; Li, L.; Pei, Q. B. *Macromolecules* **2011**, *44*, 2451.
13. Ding, J. Q.; Zhang, B. H.; Lü, J. H.; Xie, Z. Y.; Wang, L. X.; Jing, X. B.; Wang, F. *Adv. Mater.* **2009**, *21*, 4983.
14. Ge, Z. Y.; Hayakawa, T.; Ando, S.; Ueda, M.; Akiike, T.; Miyamoto, H.; Kajita, T.; Kakimoto, M. A. *Adv. Funct. Mater.* **2008**, *18*, 584.
15. Hou, L. D.; Duan, L.; Qiao, J.; Li, W.; Zhang, D. Q.; Qiu, Y. *Appl. Phys. Lett.* **2008**, *92*, 263301.

16. Jiang, W.; Duan, L.; Qiao, J.; Wang, L. D.; Zhang, D. Q.; Qiu, Y. *J. Mater. Chem.* **2010**, *20*, 6131.
17. Jiang, W.; Duan, L.; Qiao, J.; Wang, L. D.; Zhang, D. Q.; Qiu, Y. *J. Mater. Chem.* **2011**, *21*, 4918.
18. Ye, S.; Liu, Y.; Chen, J.; Lu, K.; Wu, W.; Du, C.; Liu, Y.; Wu, T.; Shuai, Z.; Yu, G. *Adv. Mater.* **2010**, *22*, 4167.
19. Gong, S. L.; Fu, Q.; Wang, Q.; Yang, C. L.; Zhong, C.; Qin, J. G.; Ma, D. G. *Adv. Mater.* **2011**, *23*, 4956.
20. Jeong, S. H.; Lee, Y. J. *Org. Electron.* **2012**, *13*, 1141.
21. Sasabe, H.; Seino, Y.; Kimura, M.; Kido, J. *Chem. Mater.* **2012**, *24*, 1404.
22. Su, S. J.; Cai, C.; Kido, J. *J. Mater. Chem.* **2012**, *22*, 3447.
23. Kim, D.; Coropceanu, V.; Bredas, J. L. *J. Am. Chem. Soc.* **2011**, *133*, 17895.
24. Fukagawa, H.; Irisa, S.; Hanashima, H.; Shimizu, T.; Tokito, S.; Yokoyama, N.; Fujikake, H. *Org. Electron.* **2011**, *12*, 1638.
25. Chaskar, A.; Chen, H. F.; Wong, K. T. *Adv. Mater.* **2011**, *23*, 3876.
26. Rothmann, M. M.; Fuchs, E.; Schidknecht, C.; Langer, N.; Lennartz, C.; Munster, I.; Strohriegl, P. *Org. Electron.* **2011**, *12*, 1192.
27. Duan, L.; Qiao, J.; Sun, Y. D.; Qiu, Y. *Adv. Mater.* **2011**, *23*, 1137.
28. Zeng, L. C.; Lee, T. Y. H.; Merkel, P. B.; Chen, S. H. *J. Mater. Chem.* **2009**, *19*, 8772.
29. Padmaperuma, A. B.; Sapochak, L. S.; Burrows, P. E. *Chem. Mater.* **2006**, *18*, 2389.
30. Burrows, P. E.; Padmaperuma, A. B.; Sapochak, L. S.; Djurovich, P.; Thompson, M. E. *Appl. Phys. Lett.* **2006**, *88*, 183503.
31. Hsu, F. M.; Chien, C. H.; Shu, C. F.; Lai, C. H.; Hsieh, C. C.; Wang, K. W.; Chou, P. T. *Adv. Funct. Mater.* **2009**, *19*, 2834.
32. Sapochak, L. S.; Padmaperuma, A. B.; Cai, X.; Male, J. L.; Burrows, P. E. *J. Phys. Chem. C.* **2008**, *112*, 7989.
33. Chou, H. H.; Cheng, C. H. *Adv. Mater.* **2010**, *22*, 2468.
34. Jiang, W.; Duan, L.; Qiao, J.; Wang, L. D.; Qiu, Y. *Org. Lett.* **2011**, *13*, 3146.
35. Ge, Z. Y.; Hayakawa, T.; Ando, S.; Ueda, M.; Akiike, T.; Miyanoto, H.; Kajita, T.; Kakimoto, M. A. *Chem. Mater.* **2008**, *20*, 2532.
36. Polikarpov, E.; Swensen, J. S.; Chopra, N.; So, F.; Padmaperuma, A. B. *Appl. Phys. Lett.* **2009**, *94*, 223304.
37. Sumalekshmy, S.; Gopidas, K. P. *J. Phys. Chem. B* **2004**, *108*, 3705.